Electronic Supplementary Material (ESI) for Soft Matter.

Supporting information: Cosolvent incorporation modulates the thermal and structural response of PNIPAM/silyl methacrylate copolymers

Jason D. Linn, Fabian A. Rodriguez, and Michelle A. Calabrese*

SI.1 Materials and methods

SI.1.1 Polymer characterization

Detailed characterization (^{1}H-NMR, ^{13}C-NMR, SEC) for all reported polymers, except for N_{783}/T_{88}, can be found in our prior report.[1] Characterization data for N_{783}/T_{88} is found below. For SEC measurements, an Agilent 1200 series HPLC equipped an Optilab T-rEX RI detector and a Wyatt DAWN HELIOS light scattering detector was used. Samples were prepared at 1 mg/mL in DMF with 50 mM LiBr and filtered through a 0.2 μm PTFE filter prior to analysis. NMR data were obtained on a Bruker Avance III HD 500 MHz spectrometer. Approximately 10 mg of polymer sample were dissolved in 800 μL of $CDCl_3$, shaken until dissolved, and then filtered through glass wool prior to analysis. 128 scans were obtained for ^{1}H-NMR and 1024 scans were obtained for ^{13}C-NMR.

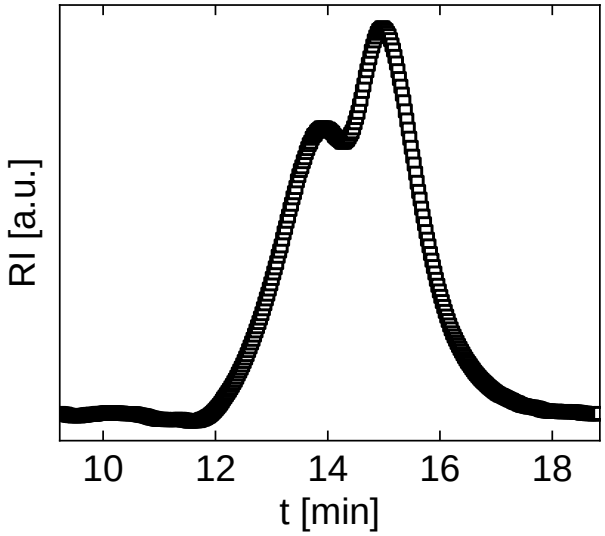

Figure S1: Size exclusion chromatography (mobile phase: DMF with 50 mM LiBr) of copolymer $N_{783}T_{88}$ with M_n = 110 kDa and $Đ$ =2.43. Large dispersity is due to silane coupling during synthesis and purification at high TMA contents ($F_{TMA} = 10.1$).

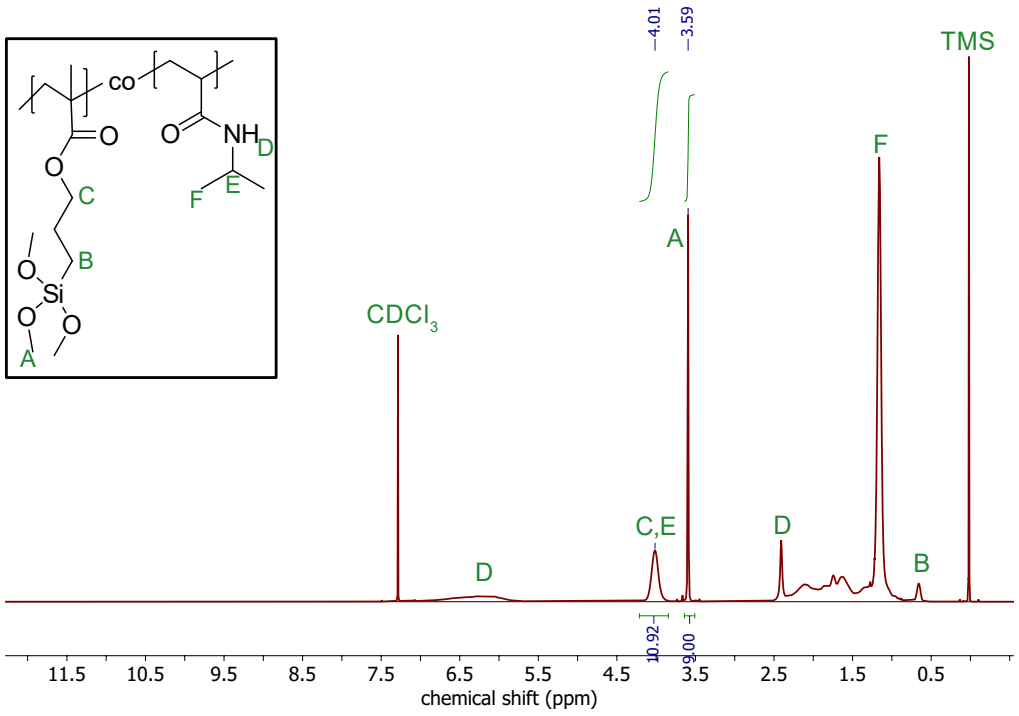

Figure S2: ^{1}H-NMR of $N_{783}T_{88}$, $F_{TMA} = 10.1\%$ mol, 500 MHz, *d*-chloroform

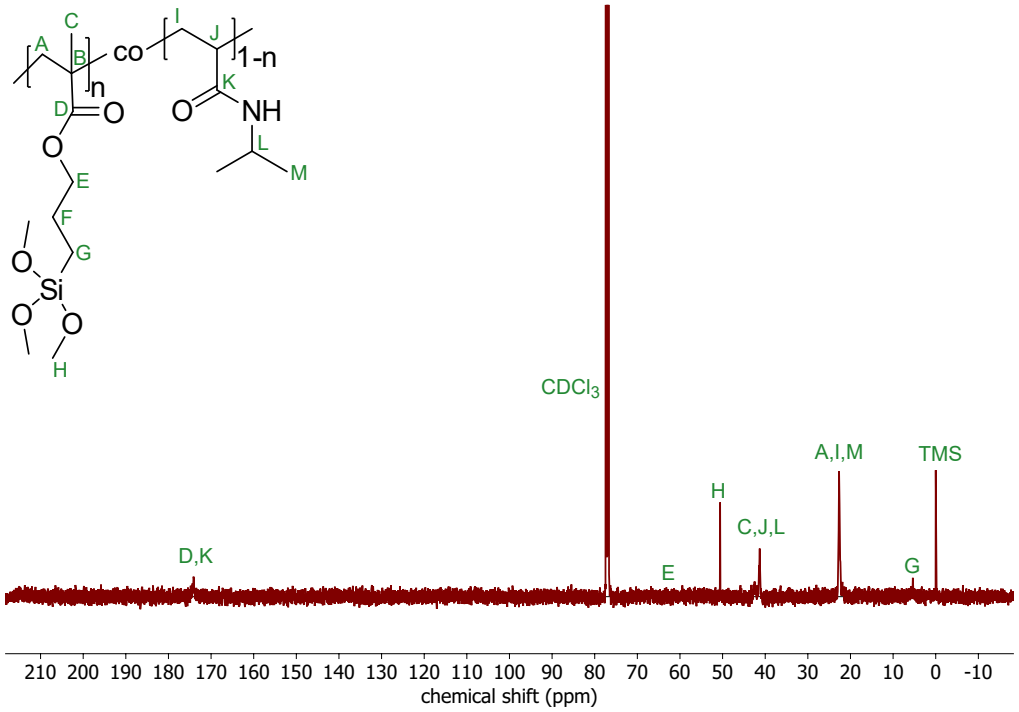

Figure S3: ^{13}C-NMR of $N_{783}T_{88}$, 126 MHz, *d*-chloroform

SI.1.2 Dynamic light scattering

The following tables contain the dispersant viscosity and refractive index values used for DLS analysis for experiments where the Malvern complex solvent builder was not used. These values have been extrapolated from literature references.[2–5]

EtOH content [% mol]	Viscosity [cP]	*n*
5	1.46	1.34
10	2.006	1.347
20	2.46	1.356
40	2.26	1.362
60	1.83	1.369

Table S1: Dispersant parameters for aqueous ethanol at 25 °C

T [°C]	Viscosity [cP]	*n*
20	1.22	1.338
25	1.07	1.337
30	0.955	1.336
35	0.846	1.336
40	0.767	1.335

Table S2: Dispersant parameters for 2% DMF

T [°C]	Viscosity [cP]	*n*
20	1.5214	1.345
25	1.3264	1.344
30	1.1214	1.343
35	1.0355	1.341
40	0.8614	1.34
45	0.8262	1.339

Table S3: Dispersant parameters for 5% DMF

SI.1.3 Cloud point testing

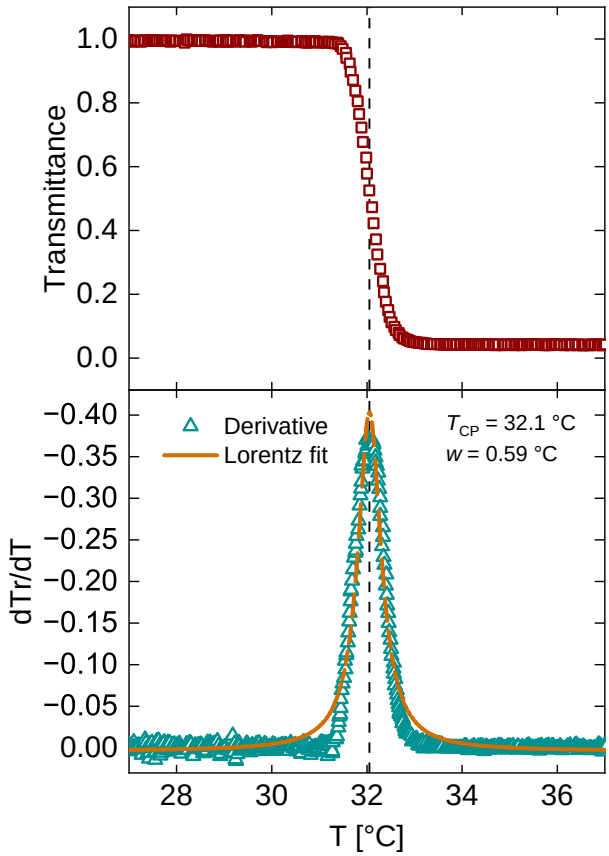

Figure S4: Example of transmittance trace from CPT (top)and subsequent analysis to determine T_{CP} or T_{Cl}, and transition width, w (bottom). The raw transmittance value is first normalized to the maximum transmittance observed in the first heating cycle, then a smoothed 1st derivative of transmittance with respect to temperature is taken (Savitsky-Golay smoothing, 51 points/bin, 3rd order polynomial). The derivative is then fit to a Lorentzian peak to extract the critical temperature and transition width.

SI.2 Results & Discussion

SI.2.1 Direct imaging of micellar structures

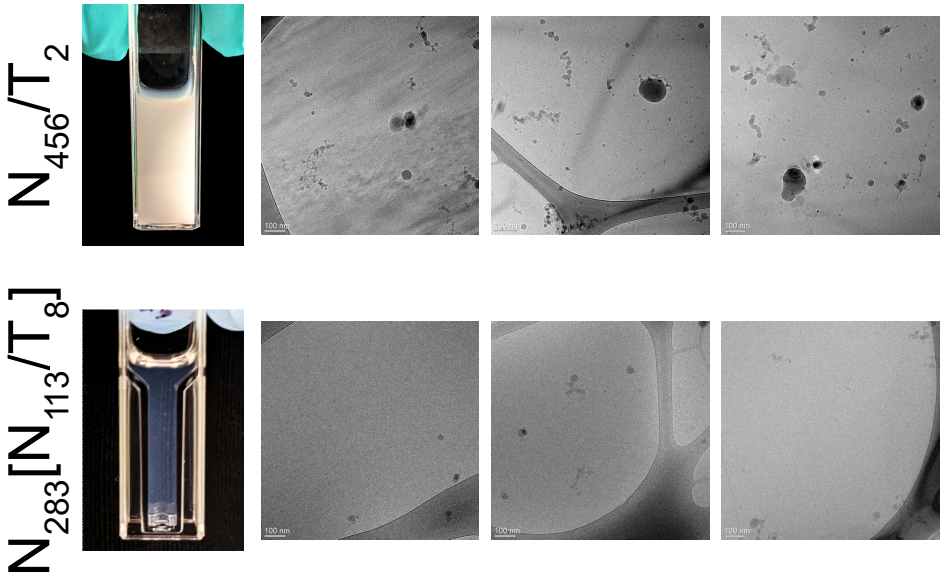

Figure S5: Direct imaging of random copolymer N_{456}/T_2, which has high D_h and broad PDI in DLS measurements, and $N_{283}[N_{113}/T_8]$, which has small D_h and PDI in DLS measurements. Heated cuvettes display strikingly different optical properties depending on the corresponding size and distribution of structures formed by the different polymer architectures. Cryo-TEM micrographs corresponding to N_{456}/T_2 show a broad range of structure sizes, including large aggregate structures and many smaller clusters. In contrast, micrographs of $N_{283}[N_{113}/T_8]$ show uniform micellar structures. Additional discussion can be found in Linn *et al.*[1] Images in this figure are reproduced from Linn *et al.*[1] with permission from the Royal Society of Chemistry.

SI.2.2 Dynamic light scattering

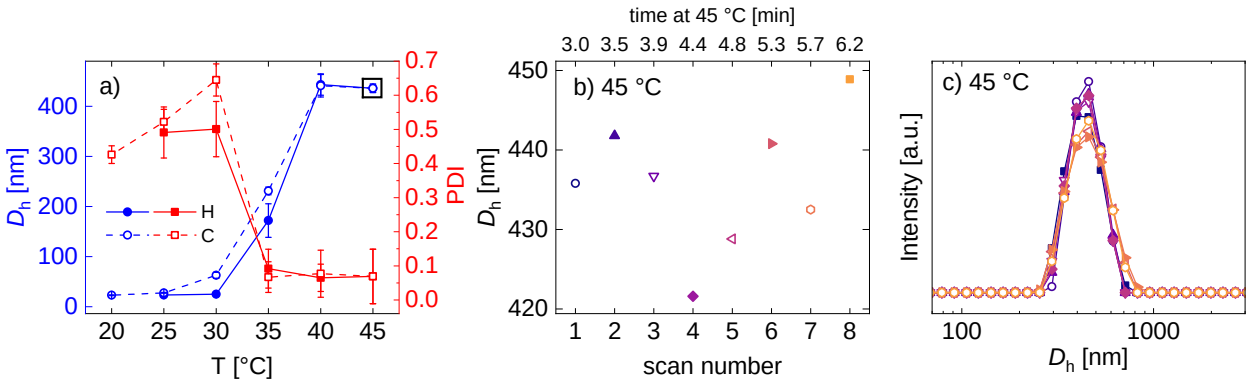

Figure S6: A typical DLS experiment control sequence used in this investigation: a) D_h (left, blue) and PDI (right, red) for $N_{293}[N_{143}/T_8]$ in 5% mol DMF across a heating and cooling cycle, where the size plateaus above T_{CP}; b) D_h versus scan number at 45 °C shows no general size trend with increasing scan number; c) intensity distributions of scans obtained at 45 °C corresponding to the values shown in b).

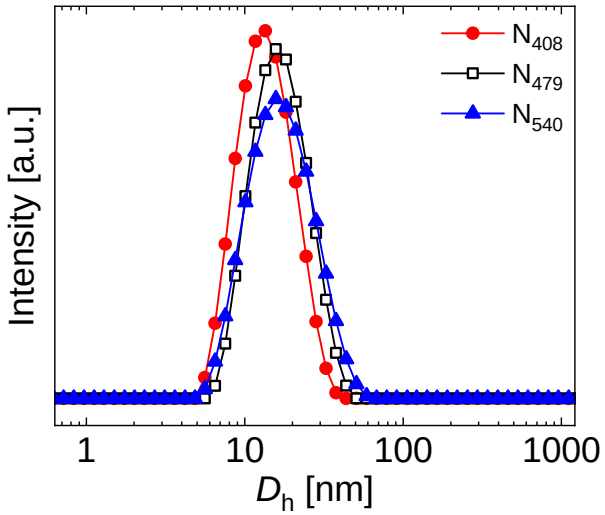

Figure S7: Intensity distribution of homopolymers of varying molecular weight do not show higher D_h clustering at room temperatures, as is observed in blocky-functional copolymers such as $N_{283}[N_{113}/T_8]$.

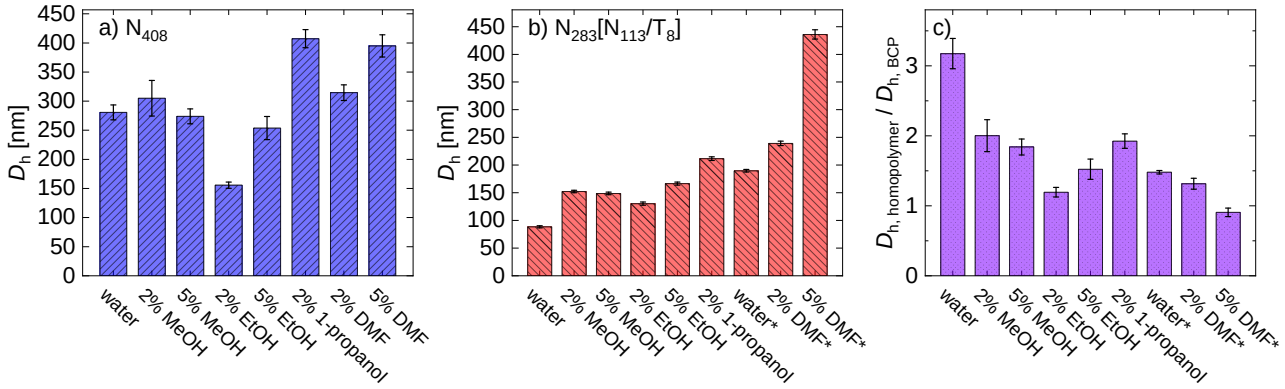

Figure S8: Solvent screening of structure sizes formed above T_{CP}. a) sizes for hompolymer N_{408}; b) sizes for blocky-functionalized copolymer $N_{283}[N_{113}/T_8]$ (* indicates data from $N_{293}[N_{143}/T_8]$); c) ratio of sizes to assess controlled structure formation (* indicates data from $N_{293}[N_{143}/T_8]$).

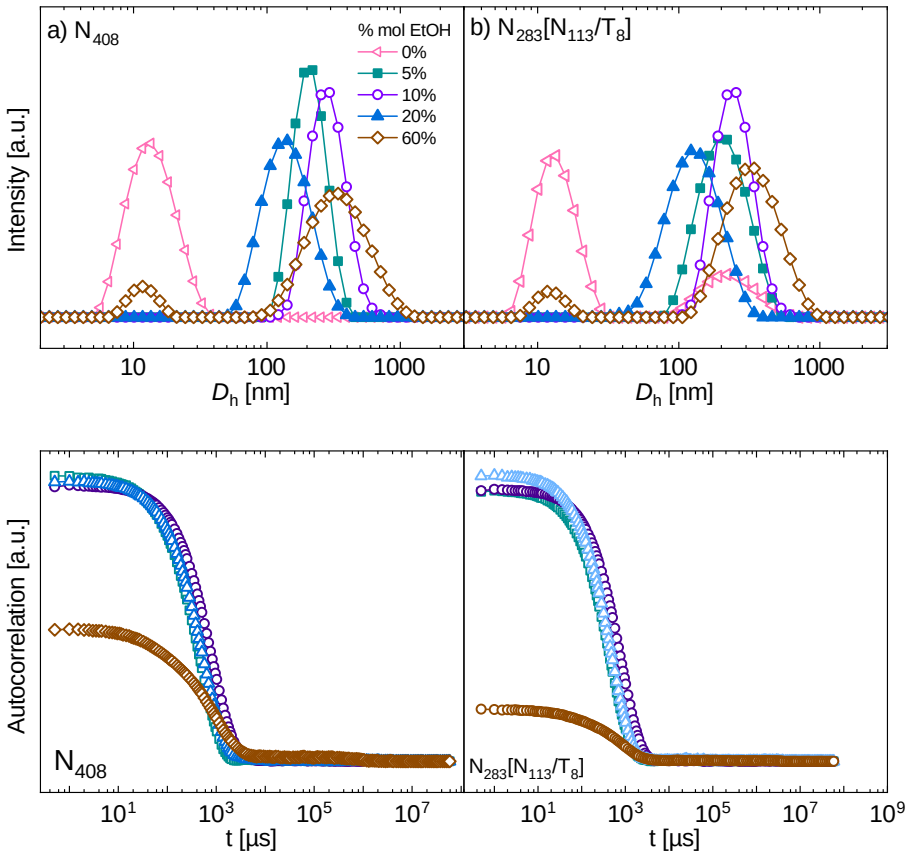

Figure S9: Intensity distributions and autocorrelation curves for N_{408} and $N_{283}[N_{113}/T_8]$ in aqueous ethanol over a range of ethanol concentrations.

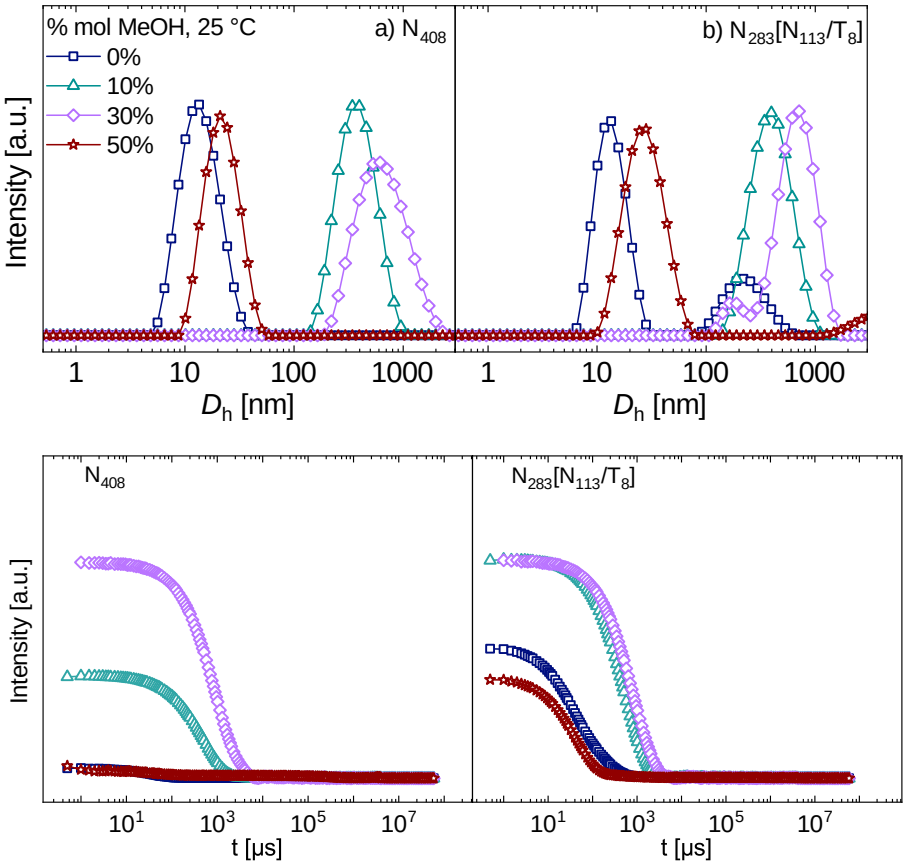

Figure S10: Intensity distributions and autocorrelation curves for N_{408} and $N_{283}[N_{113}/T_8]$ in aqueous methanol over a range of methanol concentrations.

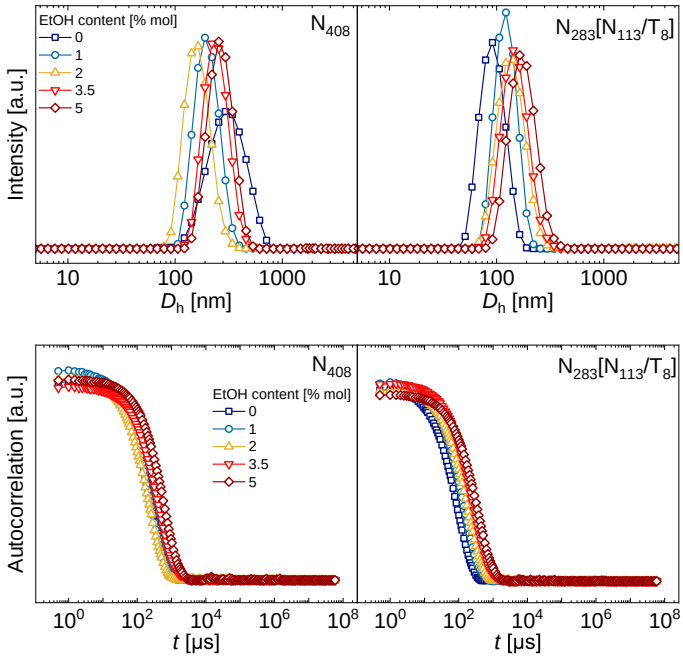

Figure S11: Intensity distribution and autocorrelation curves corresponding to Fig. 3 for N_{408} and $N_{283}[N_{113}/T_8]$ at low ethanol incorporation above T_{CP}.

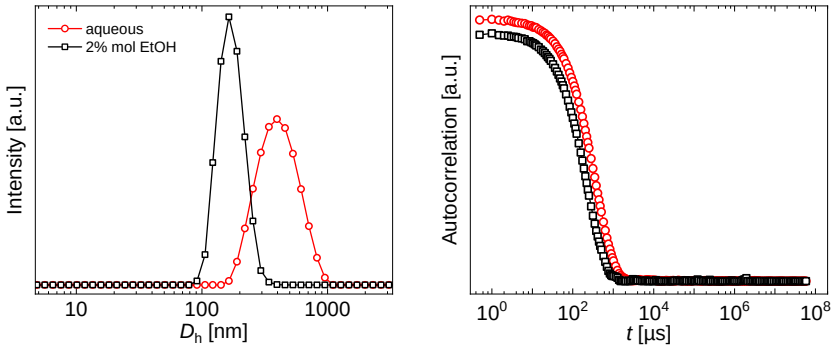

Figure S12: N_{456}/T_2 demonstrates a substantial reduction in structure size at 2% mol EtOH above T_{CP} as shown by DLS.

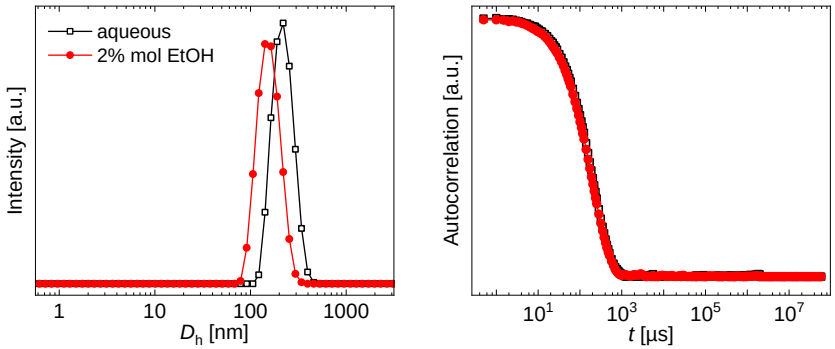

Figure S13: Intensity distribution and autocorrelation curves for N_{400}/T_{14} show a reduction in structure size at 2% mol EtOH above T_{CP}.

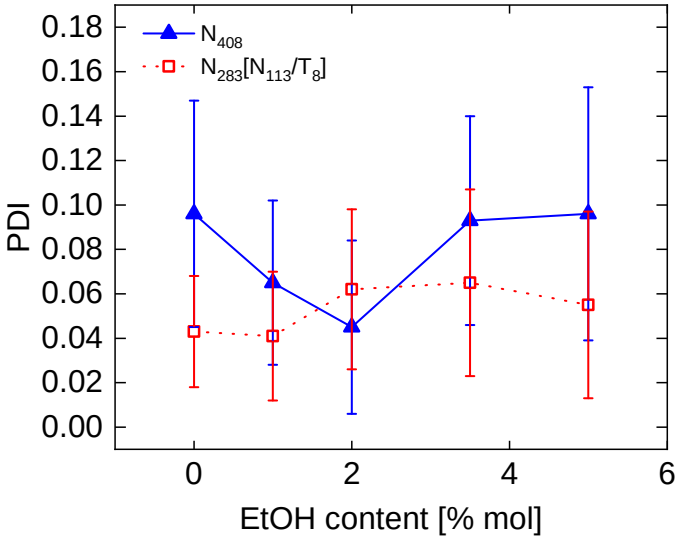

Figure S14: PDI values at $T > T_{CP}$ for homopolymer N_{408} and blocky-functionalized copolymer $N_{283}[N_{113}/T_8]$ across 0-5% mol ethanol compositions.

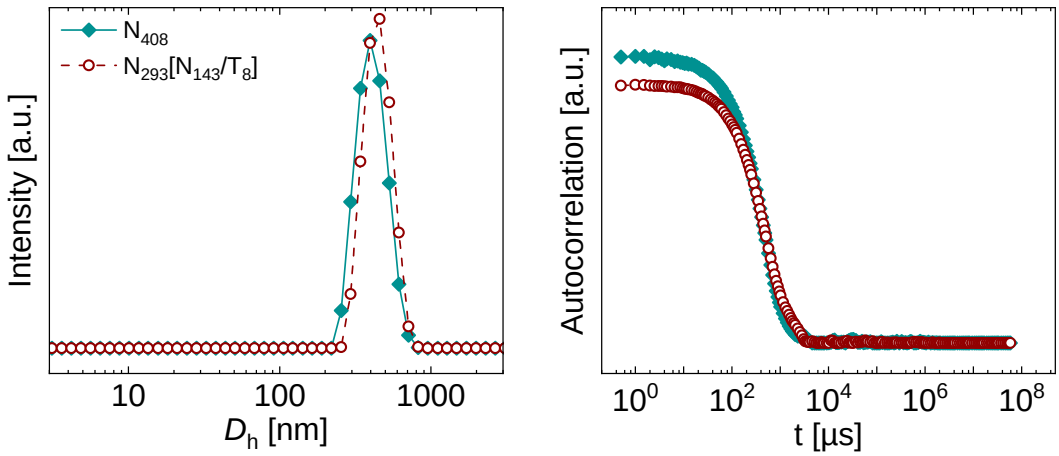

Figure S15: Homopolymer N_{408} and blocky-functionalized copolymer $N_{293}[N_{293}/T_8]$ in 5% DMF above T_{CP} display similar large sizes and disperse D_h distributions. N_{408}: $D_h = 395 \pm 19$ nm, $PDI = 0.09 \pm 0.06$; $N_{293}[N_{293}/T_8]$: $D_h = 436 \pm 8$ nm, $PDI = 0.07 \pm 0.08$.

SI.2.3 Proof-of-concept tuning of crosslinked structure sizes via cosolvent incorporation

The size of the crosslinked structures formed by N_{400}/T_{14} at high T can be tuned by altering the solvent composition. Samples of N_{400}/T_{14} were prepared at 1% wt in water. This samples was filtered through a 0.2 µm PTFE syringe filter and placed in a heat block at 45 °C for approximately 16 h. The sample was brought to room temperature, diluted with additional water to 0.1% wt and then analyzed at 25 °C with dynamic light scattering. This sample is referred to as "cured". The size of these structures compare favorably to a fresh sample that was prepared immediately prior to analysis and heated *in situ* in the DLS ("uncured").

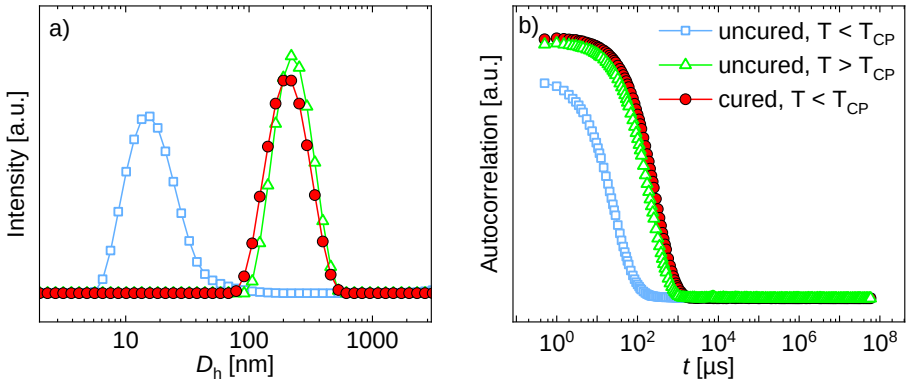

Figure S16: a) Intensity size distributions of aqueous N_{400}/T_{14} with different thermal histories, b) autocorrelation functions corresponding to traces in a). Aqueous N_{400}/T_{14} retains structure size formed at high T after substantial curing time. Fresh, uncured sample (0.1% wt polymer, blue rectangles) shows unimers when $T < T_{CP}$, when this sample is heated above T_{CP} the chains collapse and aggregate (0.1% wt polymer, green triangles). These aggregates are similar in size to a sample which has been heated to 45 °C overnight, cooled back down, and then diluted to 0.1% wt (red circles), which demonstrates that these systems can retain the large D_h structures after cooling. Additionally, the size of these crosslinked structures is similar to the aggregates formed by heating the uncured sample above T_{CP}.

Samples of N_{400}/T_{14} were prepared at 1% wt in water and in 5% mol DMF. These samples were filtered through a 0.2 µm PTFE syringe filter, then divided, and half of each was kept at 4 °C and the other half was placed in a heat block at 45 °C for approximately 16 h. The samples were brought to room temperature, diluted with additional solvent to 0.1% wt and then analyzed at 25 °C with dynamic light scattering. Samples held at cool temperatures are referred to as "uncured" and samples held at 45 °C as "cured." Compared to Fig. S16, a higher D_h peak is observed in the

uncured aqueous sample below T_{CP}, likely corresponding to some light crosslinking that occurred in the sample when held in the refrigerator overnight.

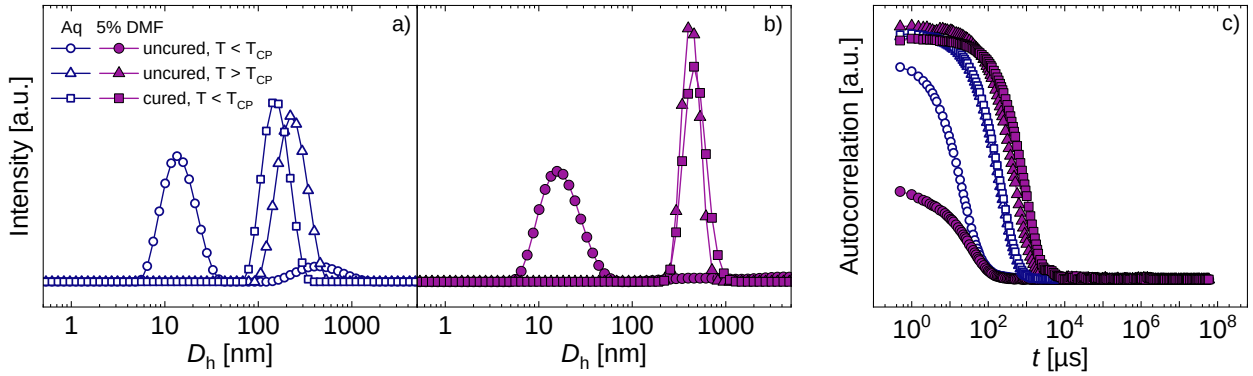

Figure S17: a) Intensity size distributions of aqueous N_{400}/T_{14} with different thermal histories, b) intensity size distributions of N_{400}/T_{14} in 5% mol DMF with different thermal histories, c) autocorrelation functions corresponding to traces in a) and b). Incorporation of cosolvent can tune the aggregate size of crosslinked structures formed from N_{400}/T_{14}. Cured structures (rectangle symbols) display substantially larger D_h at room temperature than uncured samples. While the uncured samples have similar sizes at room temperature (circle symbols, Table S4), the crosslinked structures have markedly different sizes. These structure sizes compare favorably with uncured samples that have been heated above T_{CP} (triangle symbols). Similar to prior observations (Fig. S8), a 5% mol incorporation of DMF leads to an increase in the aggregate size of uncured N_{400}/T_{14} above T_{CP}, an increase which is also observed in the cured structures at room temperature.

Sample	D_h [nm]	***PDI***
aqueous uncured, T < T_{CP}	20 ± 1.5	0.27 ± 0.01
5% DMF uncured, T < T_{CP}	15.5 ± 1	0.36 ± 0.06
aqueous uncured, T > T_{CP}	215 ± 2	0.09 ± 0.05
5% DMF uncured, T > T_{CP}	416 ± 13	0.05 ± 0.03
aqueous cured, T < T_{CP}	148 ± 2	0.07 ± 0.01
5% DMF cured, T < T_{CP}	452 ± 14	0.10 ± 0.05

Table S4: Table of D_h and PDI corresponding to distributions shown in Fig. S17. While D_h for the uncured samples are similar at room temperature, the cured samples show a drastic difference in size depending on the solvent environment while heated. These sizes are comparable to the corresponding uncured samples when heated above T_{CP}.

To validate the claim that the decrease in transmittance observed due to cycling in Fig. 5b, a cycling protocol was performed on DLS. A sample of $N_{283}[N_{113}/T_8]$ at 0.1% wt polymer in aqueous

ethanol (1% mol) was prepared. This sample was passed through glass wool and then filtered with a 0.2 µm PTFE filter. A control sequence similar to that described in Section 2.3 was used in this experiment; however, two heating and cooling cycles were performed back-to-back. A substantial reduction in D_h was observed with thermal cycling from 153 ± 2 nm on the first heating to 71 ± 1 nm on the second cycle.

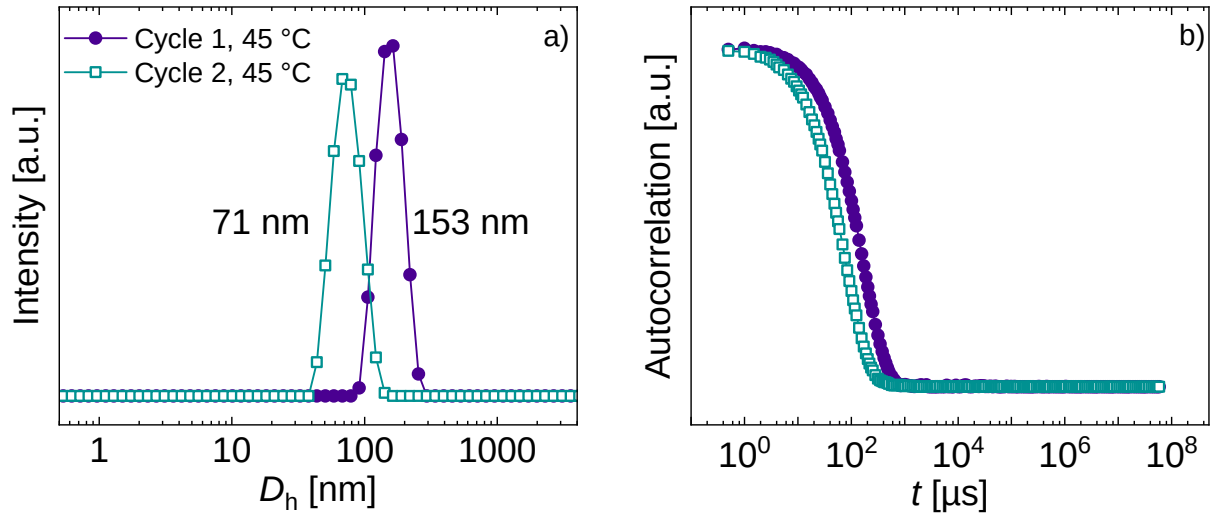

Figure S18: a) Intensity distributions of blocky-functionalized copolymer $N_{283}[N_{113}/T_8]$ at 0.1% wt polymer in aqueous ethanol (1% mol) displays a reduction in D_h at $T > T_{CP}$ from the first heating cycle to the second. b) Autocorrelation functions corresponding to traces shown in a).

To assess whether the structure size of $N_{283}[N_{113}/T_8]$ would decrease with additional time above T_{CP}, a sample was held at 45 °C overnight. This sample of $N_{283}[N_{113}/T_8]$ was prepared at 0.1% wt polymer in aqueous ethanol (1% mol) was prepared. This sample was passed through glass wool and then filtered with a 0.2 µm PTFE filter. The sample was then held at 45 °C overnight. The following day, DLS was performed to assess D_h at $T > T_{CP}$. A substantial reduction in D_h was observed in this sample, compared to a fresh sample heated for the first time, corresponding to a decrease from 153 nm to 43 nm. The results shown in Fig. S18 and Fig. S19 suggest that a stable structure size may be achieved relatively quickly, as a two fold reduction in D_h is observed on the second heating cycle. Holding the polymer sample at high T for significantly longer led to another reduction in D_h (Fig. S19); however, the difference in sizes is smaller compared to just the first and second heating cycles shown in Fig. S18.

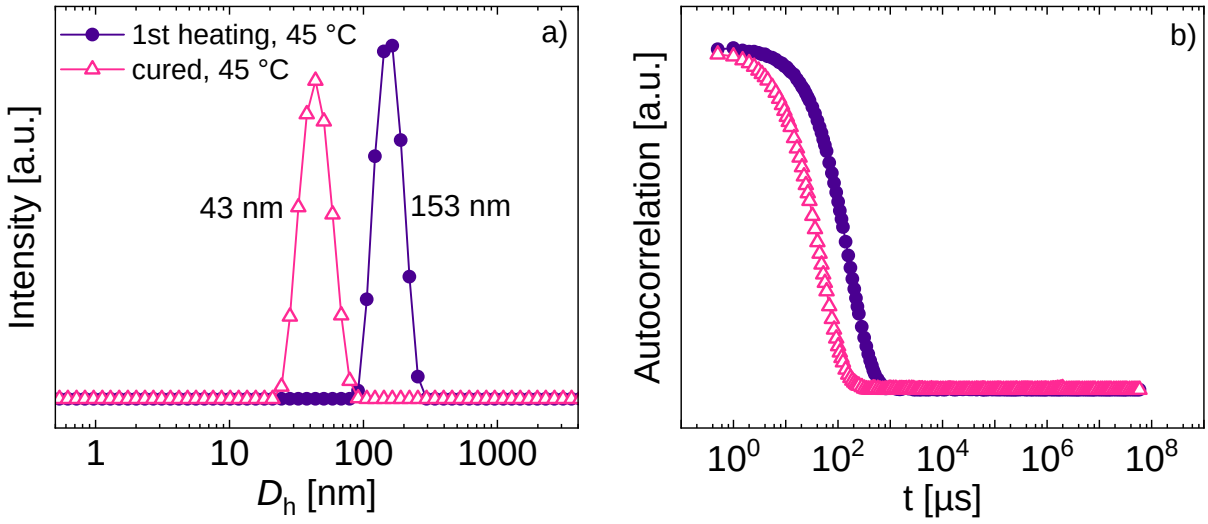

Figure S19: a) Intensity distributions of blocky-functionalized copolymer $N_{283}[N_{113}/T_8]$ at 0.1% wt polymer in aqueous ethanol (1% mol) displays a reduction in D_h at $T > T_{CP}$ after being held at high T for an extended period of time. b) Autocorrelation functions corresponding to traces shown in a).

SI.2.4 Cloud point testing

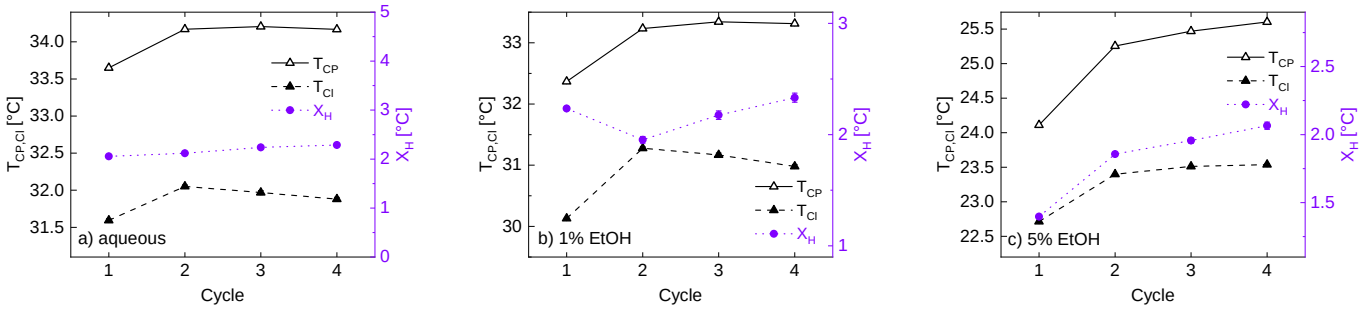

Figure S20: Cloud point temperature (T_{CP}), clearing temperature (T_{Cl}), and hysteresis parameter ($X_H = T_{CP} - T_{Cl}$) for optical responses of $N_{283}[N_{113}/T_8]$ in ethanol compositions ranging from 0 to 5% mol.

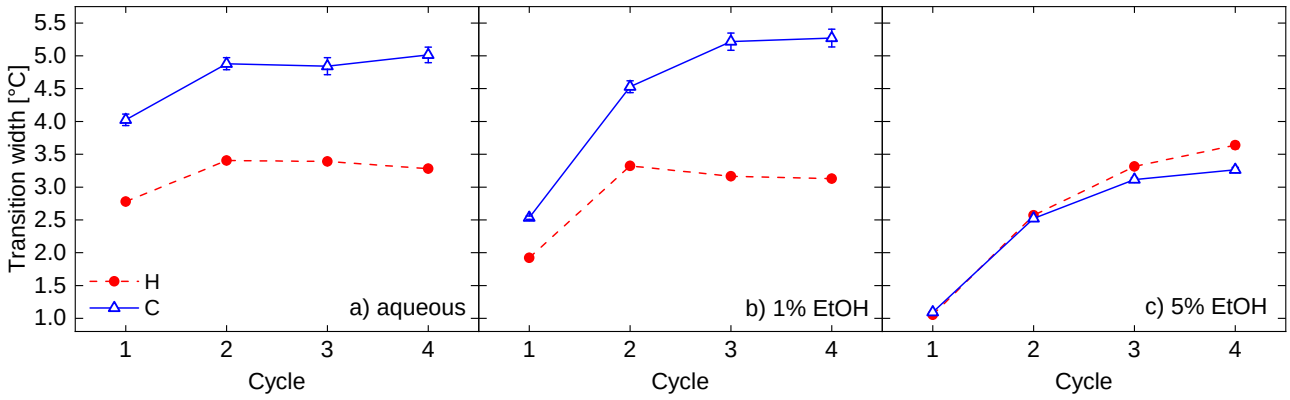

Figure S21: Transition width (w) for optical responses of $N_{283}[N_{113}/T_8]$ in ethanol compositions ranging from 0 to 5% mol.

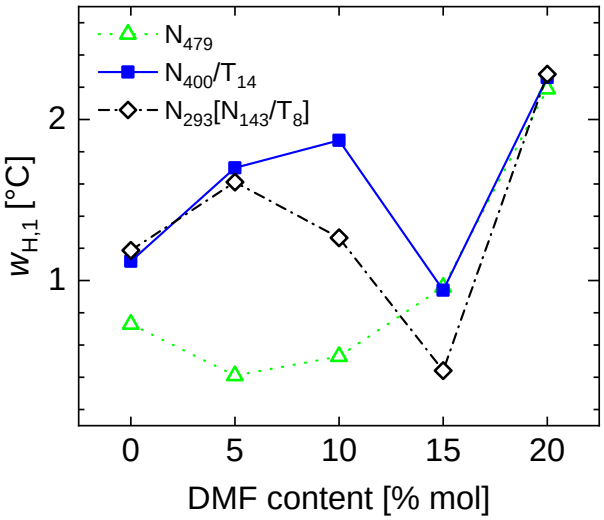

Figure S22: Transition width during the first heating cycle, $w_{H,1}$ vs. DMF content for N_{479}, N_{400}/T_{14}, and $N_{293}[N_{143}/T_8]$. Below 15% DMF, TMA incorporation leads to opposite trends in transition width compared to a homopolymer; however at and above 15% DMF, widths are similar for all polymers.

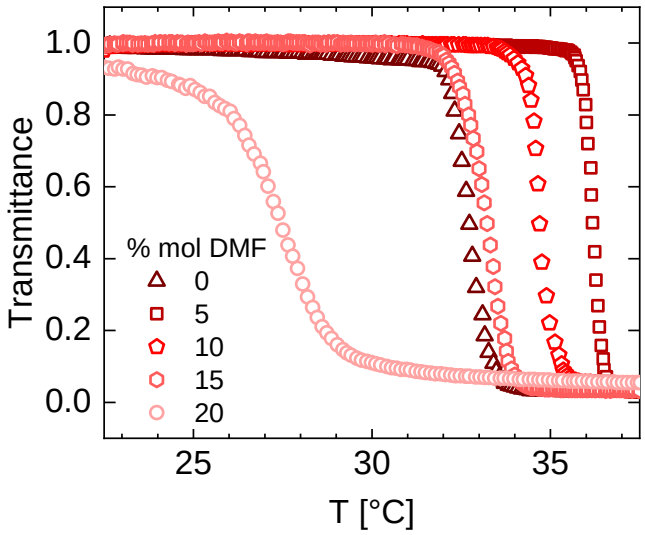

Figure S23: Optical responses of N_{479} in aqueous DMF, where DMF content primarily alters the transition temperature. Corresponding transition widths shown in Fig. S22.

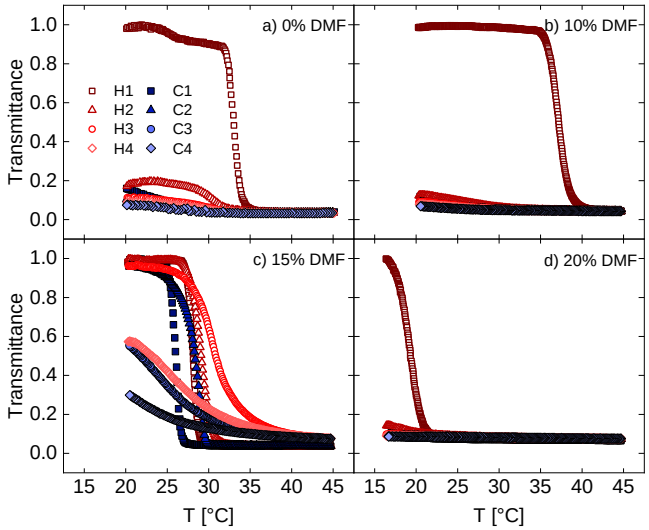

Figure S24: Optical responses of N_{400}/T_{14} in aqueous DMF, where DMF content primarily alters the transition temperature, except for the unique behavior at 15% mol DMF composition.

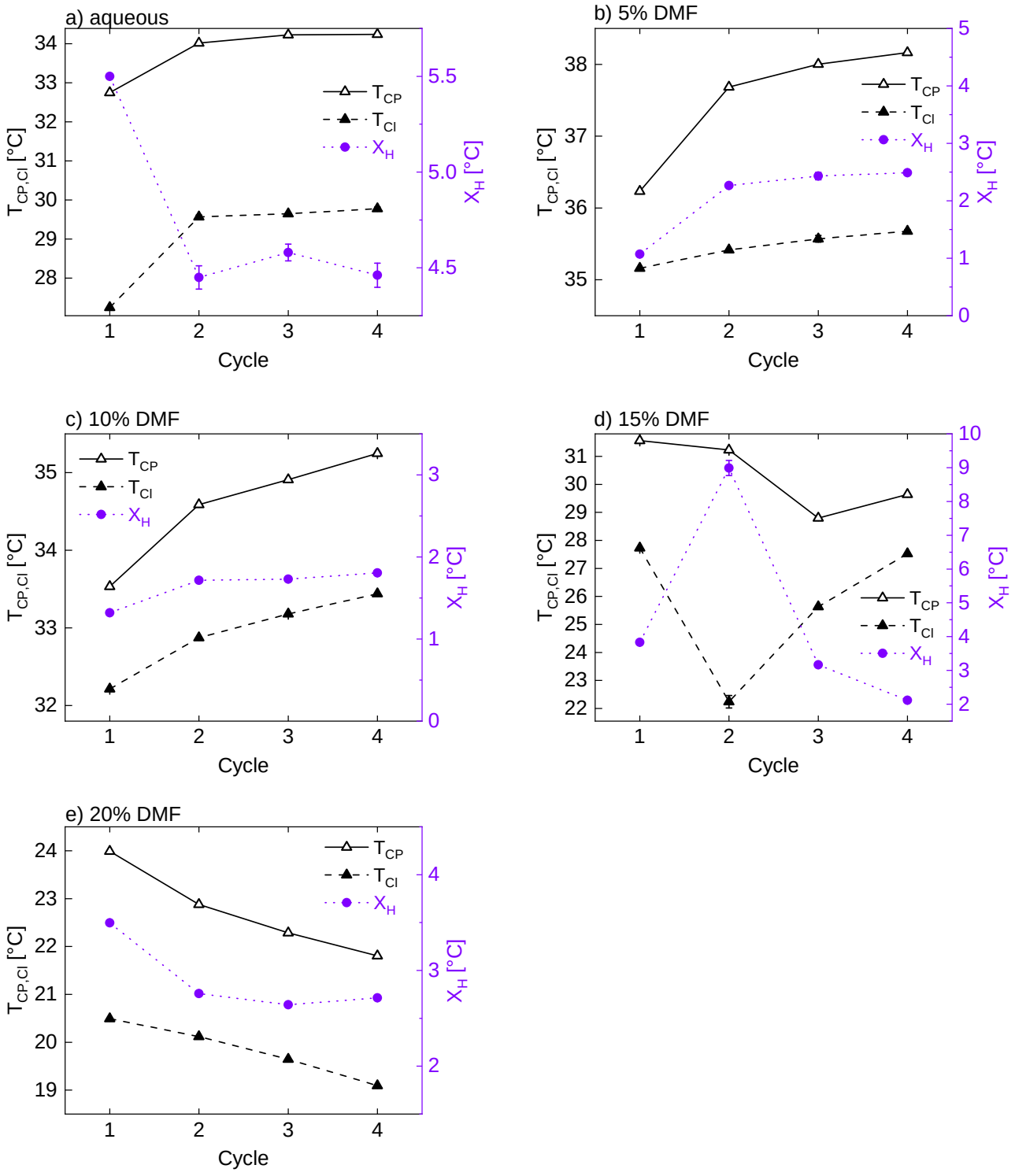

Figure S25: Cloud point temperature (T_{CP}), clearing temperature (T_{Cl}), and hysteresis parameter ($X_H = T_{CP} - T_{Cl}$) for optical responses of $N_{293}[N_{143}/T_8]$ in DMF compositions ranging from 0 to 20% mol.

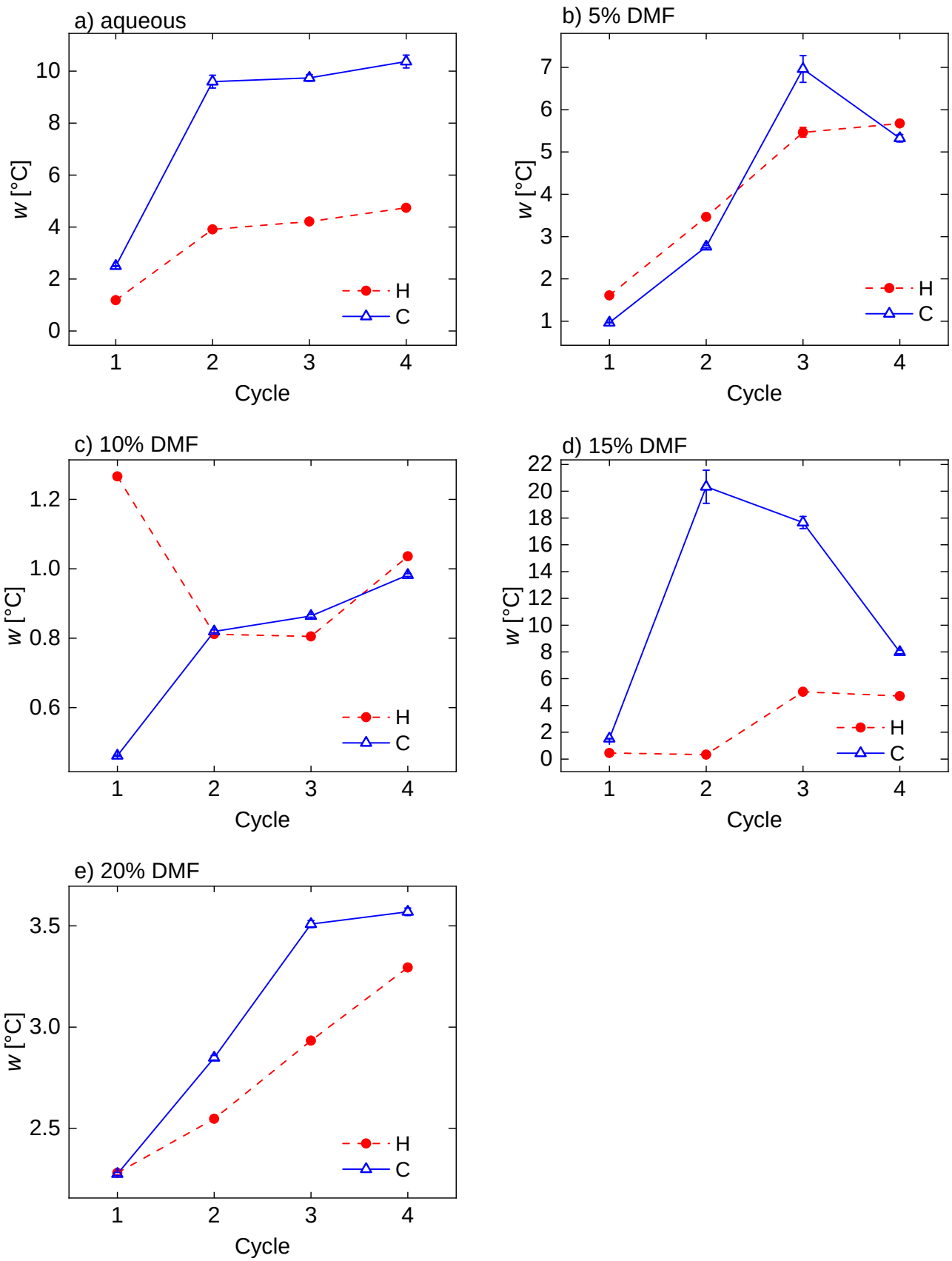

Figure S26: Transition width (w) for optical responses of $N_{293}[N_{143}/T_8]$ in DMF compositions ranging from 0 to 20% mol.

References

[1] J. D. Linn, L. Liberman, C. A. P. Neal and M. A. Calabrese, *Polymer Chemistry*, 2022, **13**, 3840–3855.

[2] F. I. El-Dossoki, *Journal of the Chinese Chemical Society*, 2007, **54**, 1129–1137.

[3] T. A. Scott, *The Journal of Physical Chemistry*, 1946, **50**, 406–412.

[4] M. Yusa, G. P. Mathur and R. A. Stager, *Journal of Chemical & Engineering Data*, 1977, **22**, 32–35.

[5] S. Taniewska-Osinska, A. Piekarska and A. Kacperska, *Journal of Solution Chemistry*, 1983, **12**, 717–727.